An Adaptive Backstepping Sliding Mode Controller to Improve Vehicle Maneuverability and Stability via Torque Vectoring Control

Lin Zhang, Haitao Ding, Jianpeng Shi, Yanjun Huang, Hong Chen, *Senior Member, IEEE*, Konghui Guo, and Qin Li

***Abstract*—To improve the maneuverability and stability of a vehicle and fully leverage the advantages of torque vectoring technology in vehicle dynamics control, a finite-time yaw rate and sideslip angle tracking controller is proposed by combining a second-order sliding mode (SOSM) controller with the backstepping method in this paper. However, existing research indicates that first-order sliding mode (FOSM) control suffers from the chattering problem, while the traditional SOSM controller requires knowing the bound of the uncertain term in advance to obtain the switching gain, which is difficult in practice. To address these problems, this paper proposes an adaptive second-order sliding mode (ASOSM) controller based on the backstepping method by adding the high-frequency switching term to the first derivative of the sliding mode variable, which implies that the actual control can be acquired after an integration process. The switching gain in the ASOSM controller is obtained by an adaptive algorithm without knowing any information of the uncertainty. The proposed algorithm is compared with FOSM and SOSM in different scenarios to demonstrate its applicability and robustness. Simulation results show that the bandwidth of the vehicle transient response can be improved by 21%. In addition, ASOSM and SOSM controllers are insensitive to vehicle mass and tire type, implying their robustness to such disturbances. Furthermore, ASOSM requires less control action because of the adaptive law when it performs similarly with SOSM and FOSM.**

Manuscript received November 10, 2018; revised May 30, 2019 and August 4, 2019; accepted September 16, 2019. Date of publication January 21, 2020; date of current version March 12, 2020. The work of Lin Zhang was supported in part by the National Natural Science Foundation of China under Grant 2017YFB0103602 and Grant U19A2069. The review of this article was coordinated by Prof. T. Shim. *(Corresponding author: Haitao Ding.)*

L. Zhang is with the Postdoctoral Station of Mechanical Engineering, School of Automotive Studies, Tongji University, Shanghai 201804, China (e-mail: zhanglin_jlu@foxmail.com).

H. Ding is with the State Key Laboratory of Automotive Simulation and Control, Jilin University, Changchun, Jilin 130025, China (e-mail: dinght@jlu.edu.cn).

J. Shi is with the Dongfeng Motor Corporation, Wuhan Economic and Technological Development Zone, Wuhan, Hubei 430058, China (e-mail: shijp@dfmc.com.cn).

Y. Huang is with the Department of Mechanical and Mechatronics Engineering, University of Waterloo, ON N2L3G1, Canada (e-mail: huangyanjun404@gmail.com).

H. Chen is with the School of Automotive Studies, Tongji University, Shanghai 201804, China (e-mail: chenhong2019@tongji.edu.cn).

K. Guo is with the KH Automotive Technologies Co, Ltd, Changchun, Jilin 130012, China (e-mail: guokh@jlu.edu.cn).

Q. Li is with the Intelligent Driving Department, GAC Automotive Research & Development Center, Guangzhou, Guangdong 511434, China (e-mail: liqin1@gacrnd.com).

Digital Object Identifier 10.1109/TVT.2019.2950219

***Index Terms*—Vehicle maneuverability and stability, torque vectoring control, sliding mode control, electric vehicle.**

I. Introduction

RISING energy costs and tightening regulations on exhaust emissions of ground vehicles stress the need for electric vehicles (EVs) [1], [2]. Although EVs may effectively address the environmental pollution and energy crises, their maneuverability and stability have consistently been a concern. It is undoubtable that when an EV is driving fast on a road surface with a low coefficient of friction, the phenomena of 'drift' and 'sharp turns' are more likely to occur, resulting in potential traffic accidents [3].

At the same time, due to the significant advantage in improving vehicle dynamics and other aspects, EVs with multiple electric motors have been attracting attention [4], [5]. Direct yaw moment can be generated by independently controlling the driving torque applied to different wheels, referring to the torque vectoring control (TVC) [6], [7]. Direct yaw moment control (DYC) is the basis of a vehicle stability control systems [8], [9]. Once such systems detect the tendency to lose stability, they will reduce the engine torque or by applying independent control of the braking force on the tires to regain the stability. However, the additional yaw moment generated by the braking method comes at the expense of reducing vehicle speed as well as drivability and brings the driver a significant sense of intervention [10]. Therefore, a stability control system based on differential braking is mainly used for emergency conditions. At the same time, the vehicle operates in the linear zone in most cases, and improving the maneuverability of the vehicle directly affects driving safety and experience [11]. However, there is consistently a difference between the actual vehicle and the vehicle model used for TVC design because of external disturbances, unknown model parameters, and unmodeled dynamics. For example, the tire cornering stiffness varies with vertical loads and is difficult to accurately estimate or measure. Therefore, in the presence of such disturbance and uncertainty, the design of a reasonable controller with the desired performance of the closed-loop system is an important part of vehicle dynamics control research. As a result, this paper focuses on the following two aspects: (1) design a TVC controller that improves the vehicle maneuverability and

stability and is robust to disturbances and parameter changes and (2) evaluate and analyze the influence of parameter uncertainty on the robustness of the designed controller by comparison with other control approaches.

The yaw rate and the sideslip angle are important parameters for describing the state of motion of the vehicle [12], [13]. The yaw rate reflects vehicle maneuverability when the sideslip angle is close to zero [14]. However, when the sideslip angle is large, for example, the vehicle drifts out of corners, and the yaw rate cannot characterize the vehicle stability because it does not reflect the trajectory of the vehicle. Consequently, it is reasonable to describe the stability of the vehicle using the sideslip angle [3]. In terms of the yaw rate controller, the coefficient of friction of a road surface must be estimated to calculate the correct reference yaw rate [15], [16]. Nevertheless, as described in reference [17], it is difficult to obtain an accurate estimate of the friction coefficient of a road without additional sensors, and the rough estimate may lead to wrongly triggering the control system or producing an unreasonable additional yaw moment. In contrast, the sideslip angle estimation algorithm has been verified by experiments and achieved good results [18], [19]. In addition to this, sideslip angle control has a better effect on vehicle stability than yaw rate control when the vehicle enters the nonlinear region [20], [21]. To counter the shortfall of the yaw rate control in the nonlinear region of the vehicle, which is heavily dependent on the friction coefficient, this paper proposes a method to control the yaw rate and the sideslip angle concurrently.

Researchers can design the appropriate TVC to achieve the expected vehicle response by different control strategy. In references [22]–[24], a nonlinear feedforward yaw moment model was used to change a vehicle's understeer characteristics under quasi-static conditions. Furthermore, a PID feedback controller was introduced to enhance the model's tracking performance under transient conditions. To obtain the optimal control law of state linear feedback, linear quadratic regulators, linear quadratic Gaussian controllers and optimal controllers were discussed in [25], [26]. However, such methods fail to consider the variation of the axle cornering stiffness of the vehicle and lack robustness to unmodeled dynamics. To fix this problem, a gain scheduling formulation that considers changes in tire cornering stiffness was incorporated into TVC [27]. The method features a simple structure and low computational complexity. In reference [28], [29], a mixed sensitivity-based H_∞ controller was designed to enhance robustness in face with external interference. Nonetheless, the approach requires more computational effort and may not meet real-time implementation requirement.

It is known that sliding mode control (SMC) possesses several advantages, such as high control precision, simple structure, and strong robustness to external disturbances and parameter perturbation under a sliding mode [30]–[32]. Therefore, in recent years, the SMC-based TVC system has received great attention. In fact, traditional FOSM technology can definitely improve the robustness of a system and the convergence speed of a controller. Nevertheless, undesirable chattering consistently arises because of the discontinuous term in the obtained control action [33]. Only when the discontinuous term is approximated by a saturation function or another continuous function will the control action not presents the high-frequency chattering [34]. Such a measure will weaken the robustness of the FOSM controller and bring obvious steady state error [35]. Nam *et al.* [36] proposed an adaptive sliding mode controller that improves yaw stability. This study validated the performance of the controller only under low vehicle speed and high friction coefficient road conditions. In reference [37], an adaptive first-order sliding mode controller (AFOSM) was designed for torque vectoring rear differential at rear axle of a SUV. The uncertainty of the cornering stiffness of the front and rear axles and the robust stability problem were studied in the paper. Wang *et al.* [38] proposed a hierarchical control algorithm to improve vehicle stability based on the adaptive siding mode control law and the trust region method. However, the chattering problem of sliding mode control is not mentioned in the paper. In order to solve the chattering problem of the first-order sliding mode, the researchers introduced second-order sliding mode control. In reference [3], direct yaw-moment control strategies were proposed for in-wheel electric vehicles using second-order sliding mode technology. A nonlinear disturbance observer was integrated into the controller to further reduce the chattering of the control action. However, the performance is still affected by the boundary of the uncertainty term. In reference [39], different feedback control structures including two typical SOSM controllers were compared.

To summarize, despite numerous theoretical studies on how to improve vehicle maneuverability and stability via TVC, no consensus has been reached regarding how to fully leverage the potential advantages of TVC. The contributions of this paper are as follows:

1) To address the shortcoming that the bound of disturbance, including system uncertainties and external disturbance, is required to obtain the switching gain in SMC, the backstepping technique and second-order sliding mode control are integrated to calculate continues control action in this paper. The unknown uncertainty of the system and the external disturbance are approximated by an adaptive law. Accordingly, the applicability and robustness of the proposed algorithm are analyzed using a dimensionless performance evaluation weighting function and are compared to other controllers in different driving scenarios, resulting in a practical new solution for the reasonable selection of a robust TVC controller. To the authors' knowledge, no study reported in the literature has done the same.
2) Most existing SMC-based TVC controllers focus on changing the understeering characteristics of the vehicle and do not improve the transient response. From the viewpoint of driving experience, excellent transient response performance is desirable because it provides a feeling of consistency to the driver and enhances drivers' perceptions of vehicle agility and driving enjoyment [40], [41]. In addition, such high-performance helps reduce the delay time of the driver-vehicle system in emergency maneuvers. Thus, a combined TVC and ASOSM method is proposed to improve the vehicle response to steering-wheel inputs under both steady-state and transient conditions and thus improve vehicle handling, active safety, and driving enjoyment.

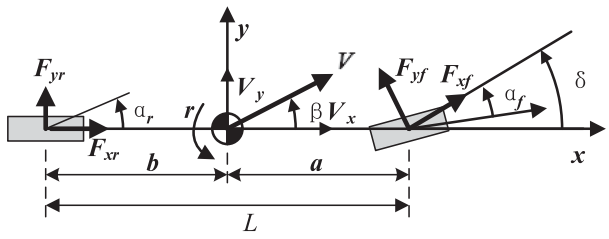

Fig. 1. 2DOF vehicle model.

II. Vehicle Dynamics and Problem Formulation

In this section, a two-degree-of-freedom (2DOF) vehicle dynamic model is used to derive the ideal yaw rate. The TVC strategy cannot be applied on the 2DOF vehicle model because the additional yaw moment ΔM_z is generated by the torque difference between the left and right wheels, while the 2DOF model treats the left and right wheels as one. Therefore, a seven-degree-of-freedom (7DOF) vehicle dynamics model is presented as well, followed by the problem statement.

A. 2DOF Vehicle Dynamic Model

As shown in Fig. 1 [42], the 2DOF vehicle dynamics model can only describe the lateral motion and yaw motion of the vehicle. Here, the model is used to calculate the ideal yaw rate, and the equations for the vehicle model are as follows:

$$\begin{cases} m(\dot{\beta}+r)V_x = (k_f+k_r)\,\beta + \left(\dfrac{ak_f-bk_r}{V_x}\right) r - k_f\delta \\ J_z\dot{r} = (ak_f-bk_r)\,\beta + \left(\dfrac{a^2k_f+b^2k_r}{V_x}\right) r - ak_f\delta \end{cases} \tag{1}$$

where V_x denotes the vehicle velocity; β refers to the sideslip angle at the vehicle's center of gravity (C.G.); δ represents the steering angle at the front wheel; a and b are the distances from the C.G. to the front and rear axle, with $L = a + b$; r represents the vehicle yaw rate; k_f and k_r indicate the equivalent cornering stiffness of the front and rear axles, respectively; and J_z is the vehicle rotational inertia around the Z-axis.

Equation (1) can be rearranged to obtain

$$\begin{cases} m\left(\dot{\beta}+r\right)V_x = Y_\beta\beta + Y_r r + Y_\delta\delta \\ J_z\dot{r} = N_\beta\beta + N_r r + N_\delta\delta \end{cases} \tag{2}$$

where

$$\begin{cases} Y_\beta = k_f + k_r; Y_r = \dfrac{ak_f-bk_r}{V_x}; Y_\delta = -k_f \\ N_\beta = (ak_f-bk_r); N_r = \dfrac{a^2k_f+b^2k_r}{V_x}; N_\delta = -ak_f \end{cases} \tag{3}$$

Following Laplace transformation, Equation (2) reads as follows:

$$\begin{pmatrix} r(s) \\ \beta(s) \end{pmatrix} = G_\delta(s)\delta(s) \tag{4}$$

$$G_\delta(s) = \begin{pmatrix} G_{\delta,r}(s) \\ G_{\delta,\beta}(s) \end{pmatrix} \tag{5}$$

where

$$\begin{aligned} G_{\delta,r}(s) &= \\ &\frac{N_\delta mV_x s + N_\beta Y_\delta - N_\delta Y_\beta}{J_z mV_x s^2 - (J_z Y_\beta + N_r mV_x)\, s - N_\beta Y_r + N_\beta mV_x + N_r Y_\beta} \\ G_{\delta,\beta}(s) &= \\ &\frac{J_z Y_\delta s + Y_r N_\delta - Y_\delta N_r - mVxN_\delta}{J_z mV_x s^2 - (J_z Y_\beta + N_r mV_x)\, s - N_\beta Y_r + N_\beta mV_x + N_r Y_\beta} \end{aligned} \tag{6}$$

$G_{\delta,r}$ is the transfer function of δ and r, where δ is the input and r is the output; $G_{\delta,\beta}$ is the transfer function of δ and β, where δ is the input and β is the output. The yaw rate dynamics can be represented by $G_{\delta,r}$.

$$G_{\delta,r}(s) = G_r \cdot \frac{1+\tau_r s}{\frac{1}{\omega_n^2}s^2 + \frac{2\zeta}{\omega_n}s + 1} \tag{7}$$

where

$$\omega_n = \frac{L}{V_x}\sqrt{\frac{k_f k_r}{J_z m}\left(1+KV_x^2\right)} \tag{8}$$

$$K = \frac{m\left(ak_f - bk_r\right)}{k_f k_r L^2} \tag{9}$$

$$\zeta = -\frac{0.5\left(J_z\left(k_f+k_r\right) + \left(a^2k_f + b^2k_r\right)m\right)}{J_z m\sqrt{\frac{ak_f-bk_r+\frac{k_f k_r L^2}{mV_x^2}}{J_z}}V_x} \tag{10}$$

$$\tau_r = -\frac{amV_x}{Lk_r} \tag{11}$$

$$G_r = \frac{V_x}{L\times\left(1+KV_x^2\right)} \tag{12}$$

In Equations (7)∼(12), K is the stability factor; ω_n and ζ are the undamped frequency and damping ratio, respectively; and G_r is the steady-state yaw rate velocity gain. Reducing K reduces the understeering of the vehicle, whereas increasing ω_n or decreasing ζ improves the vehicle transient response.

B. 7DOF Vehicle Model

In this subsection, the 7DOF dynamics of a two-wheel-drive EV are proposed. Considering the forces acting on the vehicle, as illustrated in Fig. 2, the nonlinear vehicle dynamic model with 7DOF is provided as follows [42]. The yaw motion of the vehicle can be expressed as follows:

$$\begin{aligned} J_z\dot{r} = {} & a\left(F_{yfr}+F_{yfl}\right)\cos\delta + \frac{d_f}{2}\left(F_{yfl}+F_{yfr}\right)\sin\delta \\ & - b\left(F_{yrr}+F_{yrl}\right) + \Delta M_z + \omega(t) \end{aligned} \tag{13}$$

where F_{yij} is the lateral tire force. i denotes the front or rear axle, and j is the left or right tire. δ represents the steering angle at the front wheel; a and b are the distances from the C.G. to the front and rear axle, with $L = a + b$; r represents the vehicle yaw rate; J_z is the vehicle rotational inertia around the Z-axis; ΔMz is the additional yaw moment applied to the C.G.; d_f is the track width; and $\omega(t)$ is the bounded lumped disturbance, including system uncertainties and external disturbance.

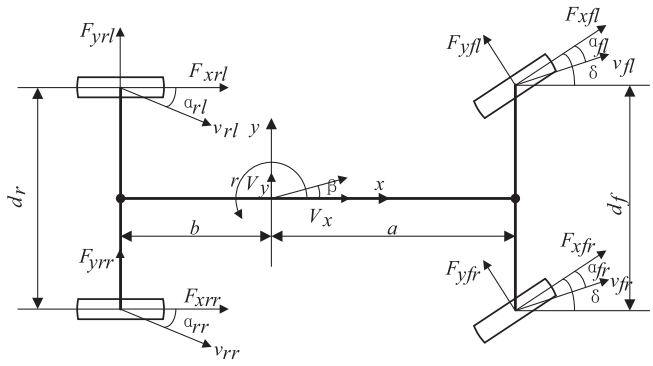

Fig. 2. 7DOF vehicle model.

Pacejka's Magic Formula is used to calculate the longitudinal and lateral tire forces. Assume that there is a frictional elliptical relationship between the peak longitudinal and lateral tire forces. For each tire, the equation for the friction ellipse is given by [43]:

$$\left(\frac{F_{xij}}{F_{xij}^{\max}}\right)^2+\left(\frac{F_{yij}}{F_{yij}^{\max}}\right)^2=1 \tag{14}$$

The maximum achievable longitudinal force is $F_{xij}^{\max}=\mu F_{zij}$, where μ is the road surface coefficient of friction and F_{zij} is the vertical load of the tire. Ignoring the pitch and roll caused by the sprung mass of the vehicle moving in the vertical direction, the vertical load of the wheel can be calculated using the static vertical load distribution and the vertical load transfer [44]. The maximum lateral force is $F_{yij}^{\max}$, and the lateral force can reach the maximum when there is no longitudinal slip. It can be expressed by the Pacejka magic formula [45].

$$F_{yij}(\alpha)=\mu F_{zij}M(\alpha) \tag{15}$$

with

$$M(\alpha)=D\sin\left\{\mathrm{Ctan}^{-1}\left[B\alpha-E\left(B\alpha-\tan^{-1}B\alpha\right)\right]\right\} \tag{16}$$

where B, C, D, E are parameters of the magic formula.

Substituting Equation (20) into Equation (19), the lateral force of the combined slip can be expressed as a longitudinal force:

$$F_{yij}=M(\alpha)\sqrt{(\mu F_{zij})^2-F_{xij}^2} \tag{17}$$

Therefore, Equation (17) is used to eliminate the lateral tire force in the model (13). The parameters B, C, D, E of the tire model (21) are fitted using a least squares estimation (LSE) method. The fitting process uses data from the tire model '205/55 R16' in CarSim. Further analysis shows that the parameters B, C, D and vertical load are linear [46]. The parameter E is omitted because it is close to zero. Therefore, they are further fitted to a linear equation:

$$\begin{aligned}B&=-8.45\times10^{-5}\times F_z+12.16428\\ C&=4.53\times10^{-7}\times F_z+1.45081\\ D&=-1.11\times10^{-5}\times F_z+1.04845\end{aligned} \tag{18}$$

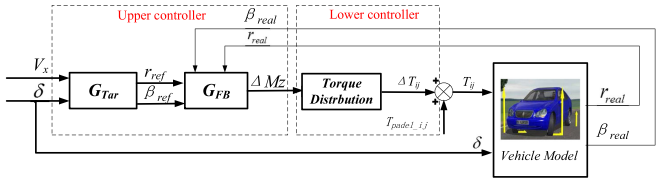

Fig. 3. Structure of TVC control system.

C. Problem Formulation

In general, vehicle inputs include the front wheel angle δ and the forces and moments applied to the vehicle C.G. To maintain the stability of the vehicle, the yaw rate and the sideslip angle must approach the desired values, which are calculated according to the 2DOF vehicle model.

In Equation (19), G_{Tar} is the target cornering response model. Equation (7) indicates that G_{Tar} can be represented via a transfer function of the second-order system. V_x and δ are imported into G_{Tar} to generate the ideal yaw rate r_t. K_{Tar},ω_{nTar} and ζ_{Tar} are the stability factor, undamped frequency and damping ratio, respectively; subscript Tar represents the vehicle parameters with TVC enabled, which will not be reiterated in the following paragraphs. K_{Tar} affects the vehicle steady steering, and reducing K_{Tar} could reduce the degree of understeering of the vehicle. The driver can negotiate curves more smoothly if the degree of understeering is reduced when entering a curve, and the degree of understeering is increased when exiting a curve [47]. Properly setting ω_{nTar} and ζ_{Tar} reduces the r response delay and improves driving safety when the driver changes lanes and avoids obstacles. Therefore, K_{Tar},ω_{nTar} and ζ_{Tar} are designed to improve the vehicle's steady-state and transient cornering responses. As indicated in reference [42], the vehicle must be in a stable state if the sideslip angle is 0. For simplicity, it is assumed herein that the ideal sideslip angle $\beta_{ref}=0$. In fact, the value does not have to be 0, as long as it is in the stable domain.

$$\begin{cases}G_{Tar}(s)=G_{rTar}\cdot\dfrac{1+\tau_r s}{\frac{1}{(\omega_{nTar})^2}s^2+\frac{2\zeta_{Tar}}{\omega_{nTar}}s+1}\\ G_{rTar}=\dfrac{V_x}{L*(1+K_{Tar}V_x^2)}\\ r_t=\delta\times G_{Tar}(s)\end{cases} \tag{19}$$

Considering that the tire force is affected by the road friction coefficient, the target yaw rate r_{ref} is limited to [3]

$$r_{ref}=\begin{cases}r_t,|r_t|\le\dfrac{0.85\mu g}{V_x}\\ \dfrac{0.85\mu g}{V_x}sign\left(r_t\right),|r_t|>\dfrac{0.85\mu g}{V_x}\end{cases} \tag{20}$$

where μ is the road adhesion coefficient.

In fact, both the yaw rate and the sideslip angle can be measured by sensors. However, many studies have focused on sideslip angle estimation due to the high cost of sideslip angle sensors. Researchers believe that accurate sideslip angle estimation can be achieved even under extreme driving conditions [7,48,49]. The structure of the TVC control system is shown in Fig. 3, and the actual yaw rate and sideslip angle

are r_{real} and β_{real}, respectively. Considering the influence of the disturbance, including system uncertainties and external disturbance, the feedback control G_{FB} is introduced, and an ideal additional yaw moment ΔM_z is generated. After the driver steps on the accelerator pedal, the desired driving torque for each tire T_{padel_ij} can be obtained which is used to control the speed of the vehicle. The torque distribution module controls the motor to generate the torque ΔT_{ij} for achieving ΔM_z. To this end, the task of this paper is to design a TVC controller that allows the actual yaw rate and sideslip angle to track their targets as closely as possible.

III. Control System Design

In this section, the control action ΔM_z will be obtained by using the SMC method. First of all, TVC controllers will be constructed by using the FOSM. Then the SOSM technique will be further applied to reduce the chattering problem existing in FOSM controllers. Finally, the ASOSM controller is proposed to obtain the switching gain without knowing any information of the uncertainty.

A. FOSM Controller Design

The first task in designing a sliding mode controller is to choose a sliding surface. The actual sideslip angle and yaw rate should track their target values. Therefore, the sliding surface can be selected as follows:

$$s = r - r_d + \rho\left(\beta - \beta_d\right) \tag{21}$$

where r_d and β_d are the target yaw rate and sideslip angle, respectively, and ρ denotes the weighting factor. When the road adhesion coefficient is small, ρ should be increased and vice versa. The choice of ρ is used to enhance or reduce the influence of the sideslip angle.

The controllability related limitations of integrated yaw rate and sideslip control, together with its potential benefits, are discussed in [20]. This paper only gives an important conclusion: when s approaches 0, the yaw rate and the sideslip angle cannot reach its target value at the same time. However, the integrated control algorithm is superior to the performance of controlling the yaw rate alone.

Finding the first derivative of (16) and substituting the result into (13) yields

$$\dot{s} = \frac{1}{J_z}\left\{a\left(F_{yfr} + F_{yfl}\right)\cos\delta + \frac{d_f}{2}\left(F_{yfl} + F_{yfr}\right)\sin\delta - b\left(F_{yrr} + F_{yrl}\right) + \Delta M_z + D_1(t)\right\} \tag{22}$$

where $D_1(t) = \omega(t) + J_z(\rho(\dot{\beta} - \dot{\beta}_d) - \dot{r_d})$. It can be concluded that $\dot{\beta}_d$ and $\dot{r_d}$ are bounded such that the constant $\bar{D}_1$ can be found such that $D_1(t) \leq \bar{D}_1$. The expression of the FOSM controller can be derived by Equation (22).

Theorem 1: If $\eta_0 > 0$ and the FOSM controller is designed to be Equation (23), the sliding surface s will converge to the origin in a limited time.

$$\Delta M_z = -J_z\eta_0 sign(s) - \left\{a(F_{yfr} + F_{yfl})\cos\delta + \frac{d_f}{2}(F_{yfl} + F_{yfr})\sin\delta - (F_{yrr} + F_{yrl})b - \bar{D}_1\,\mathrm{sign}(s)\right\} \tag{23}$$

Proof: Select Lyapunov function $V_0 = \frac{1}{2}s^2$. Taking the derivative of V_0 and combining the result with Equation (22)(23) yields

$$\begin{aligned}\dot{V}_0 &= s\dot{s} \\ &= \frac{s}{J_z}\left\{a\left(F_{yfr} + F_{yfl}\right)\cos\delta + \frac{d_f}{2}\left(F_{yfl} - F_{yfr}\right)\sin\delta - b\left(F_{yrr} + F_{yrl}\right) + \Delta M_z + D_1(t)\right\} \\ &= \frac{s}{J_z}\left\{-J_z\eta sign(s) - \bar{D}_1 sign(s) + D_1\,(t)\right\}\end{aligned} \tag{24}$$

Equation (24) can be further reduced to

$$\dot{V}_0 = \begin{cases}\dfrac{s}{J_z}\left\{-J_z\eta - \bar{D}_1 + D_1\,(t)\right\} < 0, & s > 0 \\ [2mm]\dfrac{s}{J_z}\left\{J_z\,\eta + \bar{D}_1 + D_1\,(t)\right\} < 0, & s < 0\end{cases} \tag{25}$$

According to the finite-time Lyapunov stability theory in [50], s will converge to the origin in a finite time. It is clear from *Theorem 1* that the gain of the controller (23) contains $\bar{D}_1$ to suppress the disturbance; however, $\bar{D}_1$ is difficult to obtain. To ensure the stability of the controller, $\bar{D}_1$ is usually large, resulting in a severe chattering problem. To solve this problem, a controller capable of generating a smooth control action is proposed in the following two subsections. ■

B. SOSM Controller Design

The Lyapunov direct method can be applied to the design of a traditional sliding mode control law, but for most SOSM controllers, it is very difficult to find a Lyapunov function for stability proof. Therefore, this section proposes a SOSM controller based on the combined sliding mode and backstepping design techniques such that the control action is generated in backstepping procedures.

Finding the derivative of Equation (22) yields the second derivative of s

$$\begin{aligned}\ddot{s} = \frac{1}{J_z}\Big\{&a\left(\dot{F}_{yfr} + \dot{F}_{yfl}\right)\cos\delta - a\left(F_{yfr} + F_{yfl}\right)\sin\delta\dot{\delta} \\ &+ \frac{d_f}{2}\left(\dot{F}_{yfl} - \dot{F}_{yfr}\right)\sin\delta + \frac{d_f}{2}\left(F_{yfl} - F_{yfr}\right)\cos\delta\dot{\delta} \\ &- b\left(\dot{F}_{yrr} + \dot{F}_{yrl}\right) + \Delta\dot{M}_z + \dot{D}_1(t)\Big\}\end{aligned} \tag{26}$$

Equation (26) can be expressed as

$$\ddot{s} = \alpha(t, r) + \varepsilon(t, r)\upsilon \tag{27}$$

$$\alpha(t, r) = \frac{1}{J_z}\left\{a\left(\dot{F}_{yfr} + \dot{F}_{yfl}\right)\cos\delta - a\left(F_{yfr} + F_{yfl}\right)\sin\delta\dot{\delta}\right.$$

$$+\frac{d_f}{2}\left(\dot{F}_{yfl}-\dot{F}_{yfr}\right)\sin\delta$$
$$+\frac{d_f}{2}\left(F_{yfl}-F_{yfr}\right)\cos\delta\dot{\delta}$$
$$-b\left(\dot{F}_{yrr}+\dot{F}_{yrl}\right)+\dot{D}_1(t)\Big\} \tag{28}$$

$$\varepsilon(t,r)=\frac{1}{J_z} \tag{29}$$

$$\upsilon=\Delta\dot{M}_z \tag{30}$$

where $\alpha(t,r)$ characterizes disturbance, including system uncertainties and external disturbance.

Theorem 2: If the TVC controller is designed as Equation (31), the sliding variable s and $\dot{s}$ will be stabilized to zero in a finite time.

$$\begin{cases}\Delta M_z=\int_0^t \upsilon dt=\int_0^t J_z\left(-\xi_1 s-\xi_2\dot{s}-\xi_3^{'}sign\left(k_1 s+\dot{s}\right)\right)dt\\ \xi_1=h\times k_1\\ \xi_2=c_1+h+k_1\\ \xi_3^{'}=\bar{\alpha}+\eta\\ h>0,k_1>0,\eta>0,c_1>0\\ h\left(c_1+k_1\right)-\frac{1}{4}>0\end{cases} \tag{31}$$

Proof: In the following, the backstepping method and Lyapunov stability theory are applied to prove sliding variables s and $\dot{s}$ will be stabilized to zero in a finite time given Equation (31). ■

Let $x_1=s$ and $x_2=\dot{s}$; thus, Equation (27) is rewritten as

$$\begin{cases}\dot{x}_1=s\\ \dot{x}_2=\ddot{s}=\alpha(t,r)+\varepsilon(t,r)\upsilon\end{cases} \tag{32}$$

In practical applications, $\alpha(t,r)$ has a bound, i.e., $|\alpha(t,r)|<\bar{\alpha}$. Let the target of x_1 be x_{1d}; thus, z_1 is the control error of x_1.

$$z_1=x_1-x_{1d} \tag{33}$$

$$\dot{z}_1=\dot{x}_1-\dot{x}_{1d}=x_2-\dot{x}_{1d} \tag{34}$$

Consider the following Lyapunov function:

$$V_1=\frac{1}{2}z_1^2 \tag{35}$$

$$\dot{V}_1=z_1\dot{z}_1=z_1\left(x_2-\dot{x}_{1d}\right) \tag{36}$$

It can be easily verified that if $x_2-\dot{x}_{1d}=-c_1z_1$, $c_1>0$, $\dot{V}_1$ will satisfy $\dot{V}_1\le 0$; that is, $z_1\to 0$ in a limited time. At the same time, introduce an intermediate variable z_2

$$z_2=x_2+c_1z_1-\dot{x}_{1d} \tag{37}$$

$$x_2=z_2-c_1z_1+\dot{x}_{1d} \tag{38}$$

Substituting Equation (38) into Equation (34) yields

$$\dot{z}_1=z_2-c_1z_1 \tag{39}$$

$$z_2=\dot{z}_1+c_1z_1 \tag{40}$$

Further substituting Equation (39) into Equation (36) gives

$$\dot{V}_1=z_1\dot{z}_1=z_1\left(z_2-c_1z_1\right)=z_1z_2-c_1z_1^2 \tag{41}$$

To make z_1 and z_2 approach zero, the variable τ is introduced:

$$\begin{cases}\tau=k_1z_1+z_2\\ k_1>0\end{cases} \tag{42}$$

Substituting Equation (40) into Equation (42) yields

$$\tau=\left(k_1+c_1\right)z_1+\dot{z}_1 \tag{43}$$

Obviously, if $\tau=0$, because $k_1+c_1>0$, $z_1\to 0$ and $z_2\to$ in a finite time.

The Lyapunov function V_2 is introduced:

$$V_2=V_1+\frac{1}{2}\tau^2 \tag{44}$$

$$\dot{V}_2=\dot{V}_1+\tau\dot{\tau} \tag{45}$$

Substituting Equation (43) into Equation (45) yields

$$\dot{V}_2=z_1z_2-c_1z_1^2+\tau\left(k_1\dot{z}_1+\dot{z}_2\right) \tag{46}$$

By combining Equations (37), (39), and (46), $\dot{V}_2$ takes the following form:

$$\dot{V}_2=z_1z_2-c_1z_1^2+\tau\left(k_1\left(z_2-c_1z_1\right)+\dot{x}_2+c_1\dot{z}_1-\ddot{x}_{1d}\right) \tag{47}$$

Substituting Equation (32) into Equation (47) yields

$$\dot{V}_2=z_1z_2-c_1z_1^2+\tau\left\{k_1\left(z_2-c_1z_1\right)+\alpha(t,r)+\right.$$
$$\left.+\varepsilon(t,r)\upsilon+c_1\dot{z}_1-\ddot{x}_{1d}\right\} \tag{48}$$

Substituting Equation (31) into (48) and letting $x_{1d}=0$ yields

$$\dot{V}_2=z_1z_2-c_1z_1^2-h\tau^2-h\eta\left|\tau\right|+\alpha\tau-\bar{\alpha}\left|\tau\right|$$
$$\le z_1z_2-c_1z_1^2-h\tau^2-\eta\left|\tau\right| \tag{49}$$

$\boldsymbol{Q}$ can be defined as follows:

$$\boldsymbol{Q}=\begin{bmatrix}c_1+hk_1^2 & hk_1-\frac{1}{2}\\ hk_1-\frac{1}{2} & h\end{bmatrix} \tag{50}$$

It is easy to derive the following:

$$\boldsymbol{z^T Q z}=\begin{bmatrix}z_1 & z_2\end{bmatrix}\begin{bmatrix}c_1+hk_1^2 & hk_1-\frac{1}{2}\\ hk_1-\frac{1}{2} & h\end{bmatrix}\begin{bmatrix}z_1 & z_2\end{bmatrix}^T$$
$$=-(z_1z_2-c_1z_1^2-h\tau^2) \tag{51}$$

where $\boldsymbol{z^T}=[z_1z_2]$. If $\boldsymbol{Q}$ is guaranteed to be a positive definite matrix, one can obtain the following inequality:

$$\dot{V}_2\le-\boldsymbol{z^T Q z}-\eta\left|\tau\right|\le 0 \tag{52}$$

$$\left|\boldsymbol{Q}\right|=h\left(c_1+hk_1^2\right)-\left(hk_1-\frac{1}{2}\right)^2$$
$$=h\left(c_1+k_1\right)-\frac{1}{4} \tag{53}$$

Therefore, $h(c_1+k_1-\frac{1}{4})>0$ can be obtained by selecting the values of h, c_1 and k_1, thereby ensuring that $\boldsymbol{Q}$ is a positive definite matrix and $\dot{V}_2\le 0$. According to Lyapunov stability theory and LaSalle's invariance principle proposed in reference [50], when $\dot{V}_2\le 0$, the sliding variable will realize

$x_1 \to x_{1d}$ and $\dot{x}_1 \to \dot{x}_{1d}$ in a finite time. In particular, when $x_{1d} = \dot{x}_{1d} = 0$, $x_1 = s \to 0$ and $\dot{x}_1 = \dot{s} \to 0$ will be satisfied.

However, the boundary $\bar{\alpha}$ of the disturbance is still required for the SOSM controller.

C. ASOSM Controller Design

In this subsection, the unknown uncertainty of the system and the external disturbance are addressed by an adaptive law online, eliminating the requirement of the bound of the system uncertainty in the controller design process.

Theorem 3: If the TVC controller is designed as Equations (54) and (55), then $s \to 0$ and $\dot{s} \to 0$ will be satisfied in a limited time.

$$\begin{cases} \Delta M_z = \int_0^t \upsilon dt = \int_0^t J_z \left(-\xi_1 s - \xi_2 \dot{s} - \xi_3 sign\left(k_1 s + \dot{s}\right)\right) dt \\ \xi_1 = h \times k_1 \\ \xi_2 = c_1 + h + k_1 \\ \xi_3 = \hat{\alpha}(t,r) + \eta \\ h > 0, k_1 > 0, \eta > 0, c_1 > 0 \\ h\left(c_1 + k_1\right) - \frac{1}{4} > 0 \end{cases} \tag{54}$$

$$\begin{cases} \dot{\hat{\alpha}}(t,r) = \gamma sign(k_1 s + \dot{s}) \\ \gamma > 0 \end{cases} \tag{55}$$

where $\hat{\alpha}(t,r)$ is the adaptive control law. As indicated by Equation (55), note that the proposed ASOSM has no requirement pertaining to the bound of uncertainty due to the cancellation of the term $\bar{\alpha}$.

Proof: Assume that the disturbance, including system uncertainties and external disturbance, changes slowly. Thus, Equation (56) can be derived.

$$\dot{\alpha}(t,r) = 0 \tag{56}$$

Consider the following Lyapunov function:

$$V_3 = V_2 + \frac{1}{2\gamma}\tilde{\alpha}^2 \tag{57}$$

where $\hat{\alpha}$ is the estimated value of α; the estimation error of α is

$$\begin{cases} \tilde{\alpha} = \alpha - \hat{\alpha} \\ \gamma > 0 \end{cases} \tag{58}$$

Taking the derivative of V_3 and substituting Equations (48) and (58) into Equation (47), it is obtained that

$$\begin{aligned} \dot{V}_3 &= \dot{V}_2 - \frac{1}{\gamma}\tilde{\alpha}\dot{\hat{\alpha}} \\ &= z_1 z_2 - c_1 z_1^2 + \tau\left\{k_1\left(z_2 - c_1 z_1\right) + \alpha(t,r)\right. \\ &\quad \left. + \varepsilon(t,r)\upsilon + c_1 \dot{z}_1 - \ddot{x}_{1d}\right\} - \frac{1}{\gamma}\left(\dot{\hat{\alpha}} - \gamma\tau\right) \end{aligned} \tag{59}$$

Substituting Equations (54) and (55) into Equation (59) and letting $x_{1d} = 0$, $\dot{V}_3$ can be expressed as follows:

$$\dot{V}_3 = z_1 z_2 - c_1 z_1^2 - h\tau^2 - \eta\left|\tau\right| \tag{60}$$

TABLE I
MAIN VEHICLE PARAMETERS

Symbol	Description	Value	Unit
m	Vehicle mass	1617	kg
J_z	Yaw moment of inertia	2712.4	kg· m^2
a	Front semi-wheelbase	1345	mm
b	Rear semi-wheelbase	1358	mm
h_{CG}	Height of the center of gravity	469	mm
D_f	Space between the front wheels	1475	mm
Dr	Space between the rear wheels	1500	mm
P_{D_max}	Maximum drivetrain power	160	kW
T_{D_max}	Maximum drivetrain torque	2500	Nm

According to Equation (51), Equation (60) can be written as follows:

$$\dot{V}_3 = -\boldsymbol{z}^{\boldsymbol{T}}\boldsymbol{Q}\boldsymbol{z} - \eta\left|\tau\right| < 0 \tag{61}$$

The design of $\boldsymbol{Q}$ is the same as that of Equation (53).

ΔM_z needs to be achieved by the motor torque ΔT_{ij}:

$$\begin{aligned} \Delta T_{fl} &= \Delta T_{rl} = -\frac{\Delta M_z}{d_f R_e} \\ \Delta T_{fr} &= \Delta T_{rr} = \frac{\Delta M_z}{d_f R_e} \end{aligned} \tag{62}$$

where R_e is the wheel radius. ■

IV. CASE STUDY

A standard CarSim B-Class vehicle in CarSim is selected as the target vehicle, and a rear-wheel driven electric vehicle with two in-wheel motors is taken as an example. The key parameters of the vehicle are shown in Table I. The Simulink-CarSim collaborative simulation provides the simulation environment for the test control system and validates the algorithm under double lane change (DLC) conditions and ramp steer tests.

A. DLC Under High-Adhesion Road Conditions

The ASOSM algorithm is verified under DLC conditions, with $\mu = 0.8$. Vehicle speed is essentially maintained at approximately 80 km/h, that is, $V_x = 80$ km/h. When the TVC is turned off, the stability factor $K_{ori} = 2 \times 10^{-3}$ of the vehicle at $V_x = 80$ km/h is obtained by identification, the undamped natural frequency is $\omega_{ori} = 0.98$ Hz, and the damping ratio $\zeta_{ori} = 0.75$. To improve the transient response of the vehicle, the target undamped frequency and the damping ratio are set to $\omega_{nTar} = 1.29$ Hz and $\zeta_{Tar} = 0.75$. In addition, proper reduction of understeering of the vehicle can help the driver use a smaller steering wheel angle to pass a corner; thus, the target stability factor is set to $K_{Tar} = 2 \times 10^{-4}$. The parameters of the control algorithm are shown in Table II.

In Fig. 4, as ρ increases from 0 to 4, the tracking error of the yaw rate increases. When $\rho = 0$, the following error of the yaw rate is smaller than that when $\rho = 3$ because the additional yaw moment is mainly used to suppress the sideslip angle. Typical case are shown in E1 and E2 of Fig. 4.

The bandwidth f_{pb} is used to evaluate the system's transient response performance. A high f_{pb} means that the system is

TABLE II
CONTROL ALGORITHM PARAMETERS WHEN THE TVC IS TURNED ON OR OFF

TVC Off	TVC On
$K_{ori} = 2 \times 10^{-3}$ $\omega_{ori} = 0.98Hz$ $\zeta_{ori} = 0.75$	$K_{Tar} = 2 \times 10^{-4}$ $\omega_{nTar} = 1.29Hz$ $\zeta_{Tar} = 0.75$
-	$h = 2,\ k_1 = 0.5,\ c_1 = 0.5,\ \eta = 0.1,\ \gamma = 0.1$

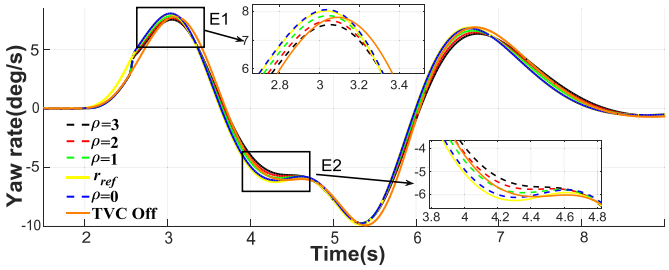

Fig. 4. Yaw rate under different ρ.

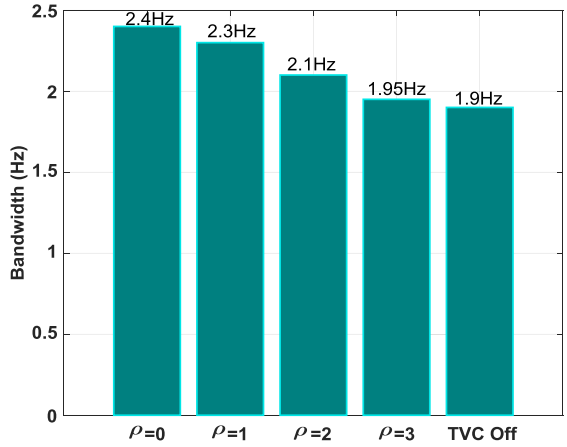

Fig. 5. Bandwidth under different ρ.

highly capable of adapting to different frequency signals and that the system exhibits a fast response under a high-frequency input. As shown in Fig. 5, f_{pb} gradually increases as ρ decreases. When $\rho = 0$, $f_{pb} = 2.4$ Hz, the maximum value. In other words, the system's transient responsiveness can be increased by 21% when the TVC is turned on.

As shown in Fig. 6, when the TVC is turned on, as ρ decreases, the vehicle trajectory progressively approaches the target path. Compared with that when the TVC is off, the vehicle trajectory in the case of $\rho = 0$ is closer to the target path, as indicated by Y1 and Y2 in Fig. 6. The response of the steering wheel angle is shown in Fig. 7. As ρ decreases, the steering wheel angle decreases in sequence at the peak (as indicated by S1 $\sim$ S3 in Fig. 7). Compared with the case in which the TVC is off, when $\rho = 0$, the driver can use a smaller steering wheel angle to drive closer to the target path, which not only improves the vehicle's maneuverability but also enhances driving pleasure and makes it easier for the driver to pass corners.

Fig. 8 clearly shows that as ρ increases, the peak value of β decreases. When the TVC is turned off, the peak value of β is smaller than that when $\rho = 0$, $\rho = 1$ and $\rho = 2$, but greater than

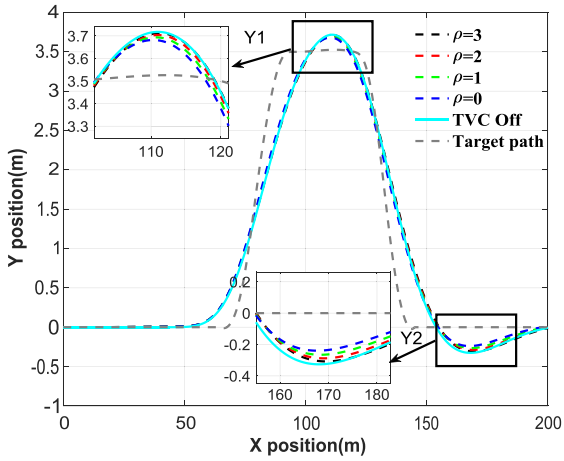

Fig. 6. Vehicle trajectory under different ρ.

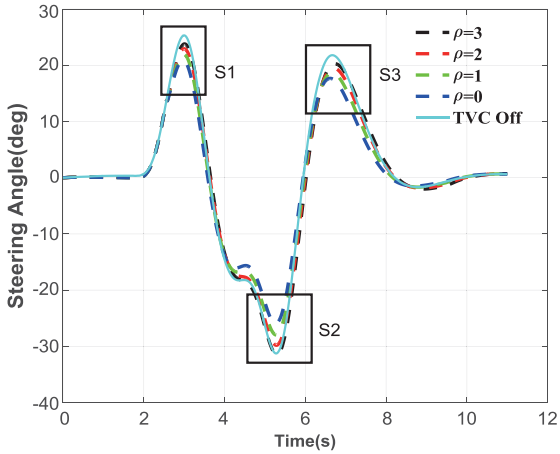

Fig. 7. Steering angle under different ρ.

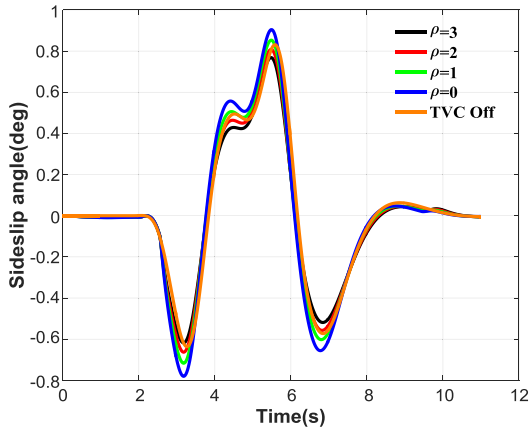

Fig. 8. Sideslip angle under different ρ.

the value at $\rho = 3$. That is, although the vehicle maneuverability can be improved by setting K_{Tar}, ω_{nTar}, and ζ_{Tar}, doing so also affects vehicle stability.

In this paper, the $\beta - \dot{\beta}$ phase plane analysis method is used to further analyze vehicle stability. If the phase trajectory of the sideslip angle starts from the initial point and ultimately returns to the origin, the vehicle is consistently stable throughout the

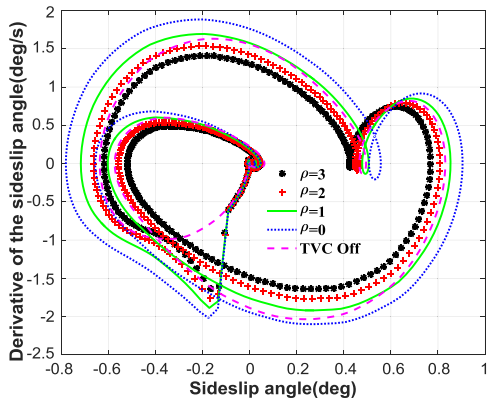

Fig. 9. Phase trajectory of sideslip angle under different ρ.

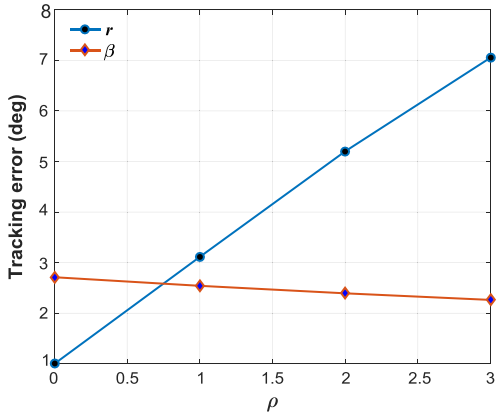

Fig. 10. Yaw rate and sideslip angle of tracking error under different ρ.

driving process. In addition, the smaller the area of the phase trajectory on the phase plane is, the more stable the vehicle becomes [6]. The phase trajectory of the sideslip angle is shown in Fig. 9. The vehicle is consistently stable regardless of whether the TVC is turned on. As ρ increases, the area of the phase trajectory on the phase plane decreases, and the stability of the vehicle is enhanced. When $\rho = 3$, the area of the phase trajectory on the phase plane is smaller than when the TVC is turned off; that is, the vehicle stability can be improved by changing the control parameter ρ.

As shown in Fig. 10, as ρ increases, the error of the yaw rate increases, while the error of the sideslip angle decreases. Thus, the maneuverability and stability of the vehicle can be balanced by properly setting $K_{Tar}, \omega_{nTar}, \zeta_{Tar}$, and ρ without changing the mechanical parameters of the vehicle. For example, for drivers with aggressive driving styles, maximally improving vehicle maneuverability based on the premise of keeping the vehicle stable could make driving more enjoyable. In this case, ρ can be set to 0. For drivers with a conservative driving style, as long as the vehicle is stable, we can set $\rho = 3$.

B. DLC Under Low-Adhesion Road Conditions

In this subsection, FOSM, SOSM and ASOSM controllers are compared and evaluated by proposed evaluation index. Robustness is assessed by varying the vehicle weight and considering the two different tire types.

1) Evaluation Index of Controller Performance: According to the requirements of the international DLC test, ISO 3888-2:200, $\mu = 0.2$ and $V_x = 80$ km/h are set. Under this condition, tires operate in the nonlinear zone in most cases. This section compares the control performance of different control algorithms under low-adhesion road. The dimensional performance evaluation weighted function $DPEF$ is built to evaluate the control performance of the algorithm [39].

Control error $e_r = r_{real} - r_{ref}$, $e_\beta = \beta_{real} - \beta_{ref}$, the tracking error of the i-th vehicle travel track point $e^i_{tra} = Y^i_{real} - Y^i_{ref}$, and control action ΔM_z are used to evaluate the performance of the algorithm, where Y^i_{real} and Y^i_{ref} are the i-th ordinates of the actual travel track point and the target path point ordinate in the geodetic coordinate system, respectively.

- The integral of the absolute value of the control error:

$$IACE = \int_0^{t_m} (|e_r| + |e_\beta|)dt \tag{63}$$

- The integral of the product of the absolute value of time and error:

$$IATE = \int_0^{t_m} t_m(|e_r| + |e_\beta|)dt \tag{64}$$

- The accumulation of the absolute value of vehicle trajectory tracking error:

$$AATE = \sum_{i=1}^{n} e^i_{tra} \tag{65}$$

- The integral of the absolute value of the control action:

$$IACA = \int_0^{t_m} |\Delta M_z|\, dt \tag{66}$$

where t_m is the duration of the TVC.

The *ITTE* complements the *IACE*. For example, minimizing the *IACE* in a step steer will reduce the system's overshoot but requires a longer settling time because the *IACE* does not consider the time factor [51]. To evaluate the performance of different controllers in a simple and objective manner, *DPEF* is defined as follows:

$$\begin{aligned} DPEF = &\frac{\omega_1}{\max(|r|, |\beta|)\, t_m} IACE \\ &+ \frac{\omega_2}{\max(|r|, |\beta|)\, t_m^2} IATE \\ &+ \frac{\omega_3}{(AATE_{th})} AATE + \frac{\omega_4}{\Delta M_{z\max} t_m} IACA \end{aligned} \tag{67}$$

where ω_1, ω_2, ω_3 and ω_4 are the weights of the *IACE*, *IATE*, *AATE* and *IACA*, respectively, and $\omega_1 + \omega_2 + \omega_3 + \omega_4 = 1$. $\max(|r|, |\beta|)$ is the absolute value of the maximum value that r and β can achieve under the proposed maneuver, which can be set to 0.2. $AATE_{th} = 2000$ is the threshold of the $AATE$. $\Delta M_{z\max}$ is the maximum feasible absolute value of the additional yaw moment. To evaluate whether the control algorithm could use

TABLE III
TIRE PARAMETERS

Symbol	Description	Quantity
-	Tire A	185/65/R15
-	Tire B	185/55/R16
k_f	Cornering stiffness at $F_{z,Norm}$ (Tire A)	7.3115E+04N/rad
k_f	Cornering stiffness at $F_{z,Norm}$ (Tire B)	8.5045E+04N/rad
$F_{z,Nom}$	Nominal vertical force	5500N
$F_{y,max}$	Maximum lateral force at $F_{z,Norm}$ (Tire A)	5094N
$F_{y,max}$	Maximum lateral force at $F_{z,Norm}$ (Tire B)	5339N

TABLE IV
CONTROL PARAMETERS

Controllers	Parameters
FOSM (23)	$\rho = 0$, $\eta_0 = 0.1$
SOSM (31)	$\rho = 0$, $h = 2$, $k_1 = 0.5$, $c_1 = 0.5$ $\eta = 0.1$, $\bar{\alpha} = 0.5$
ASOSM (54)(55)	$\rho = 0$, $h = 2$, $k_1 = 0.5$, $c_1 = 0.5$ $\eta = 0.1$, $\gamma = 0.1$

a smaller ΔM_z in a short time to track the r_{ref}, β_{ref} and the target path, $\omega_1 \sim \omega_4$ are set to 0.25.

Different tests are simulated using the CarSim vehicle model. Robustness is assessed by varying the vehicle weight and considering the two different tire types indicated in Table III. To ensure vehicle stability on a low-adhesion road surface, a large understeering degree and bandwidth are obtained by setting $K_{Tar} = 2 \times 10^{-3}$, $\omega_{nTar} = 1.29$ Hz, and $\zeta_{Tar} = 0.75$. The parameters of the different control algorithms are shown in Table IV.

2) Simulation Results for Different Controllers: Because $\rho = 0$, the controller only considers the response of the yaw rate r. The simulation results are shown in Fig. 11∼Fig. 13 for Tire A and $m = 1617$ kg. When the TVC is turned off, r_{real} deviates significantly from r_{ref}. When the TVC is turned on, the three algorithms overshoot at Time $= 2.2$ s, as shown in Fig. 11 b $\sim$ d. In addition to overshooting, the FOSM controller exhibits a large amount of chattering (F in the Fig. 11b), which causes the vehicle to be unstable and gives the driver a poor driving experience. As shown in Fig. 11b, due to the inability to accurately determine $\bar{\alpha}$, in addition to the large overshoot at O1, the SOSM controller shows a slow convergence speed at O2. Compared to the FOSM and SOSM controllers, the ASOSM controller has a small overshoot at A in Fig. 11d. Under the effects of the adaptive law and the integration of $\Delta \dot{M}_z$, the ASOSM controller shows neither the chattering nor a slow convergence.

The vehicle trajectory is described in Fig. 12, and it can be clearly observed that when the TVC is turned off, the vehicle trajectory seriously deviates from the target path such that the driver cannot control the direction of the vehicle. However, the three sliding mode controllers designed in this paper can make the vehicle trajectory follow the target path well. Among them, the FOSM and ASOSM controllers exhibit higher tracking accuracy than does the SOSM controller.

The yaw rate r reflects the driver's intention, that is, whether the vehicle can operate in accordance with the driver's expected path, while the sideslip angle β reflects the vehicle's stability. For vehicle stability control, r and β are equally important. The sideslip angle control in the TVC can only change the longitudinal and lateral forces of the tires by controlling the longitudinal force of each tire; however, it is difficult to achieve precise control of the lateral force. Therefore, the sideslip angle is suppressed in the stable region and cannot be zero. In Fig. 13, the maximum value of β is approximately 5.2 deg when the TVC is turned off, which is also the reason for the vehicle's instability. The three controllers designed in this paper can suppress β in the range of -1.5 deg$\sim$1.5 deg and maintain vehicle stability. The peak value of β for the SOSM controller is the smallest (T in the Fig. 13). Fig. 12 shows that, although the application of the SOSM controller can reduce β and maintain vehicle stability, it also generates a large trajectory tracking error. Therefore, the performance of the controller cannot be evaluated based solely on β.

Curves of the additional yaw moment ΔM_z are depicted in Fig. 14. The FOSM controller output has a large peak value and chattering (Y1 in the Fig. 14), and the maximum value of ΔM_z is approximately 2350 N. In contrast, the maximum values of ΔM_z for the ASOSM and SOSM controllers are 2100 N and 2480 N, respectively (Y2 in Fig. 14), and ΔM_z changes smoothly. In other words, the ASOSM controller can reduce the requirement of the peak output torque of the actuator and solve the chattering problem of the FOSM controller.

The controller's performance evaluation index, $DPEF$, is shown in Fig. 15. By changing the tire parameters and vehicle mass at the same time, the degree of variation of $DPEF$ can be expressed as the percentage P_{FOSM} of $DPEF$ increase or decrease:

$$P_{FOSM} = \left| \frac{\max(DPEF) - \min(DPEF)}{\max(DPEF)} \right| \times 100\% = 17.39\% \tag{68}$$

Similarly, $P_{SOSM} = 16.67\%$ and $P_{ASOSM} = 4.44\%$. Therefore, the ASOSM and SOSM controllers are insensitive to vehicle weight and tire type and exhibit strong robustness. In contrast, the performance of the FOSM controller is sensitive to tire type and insensitive to vehicle weight. It should be emphasized that the ASOSM controller consistently achieves the minimum $DPEF$ regardless of the tire parameters or vehicle mass, i.e., the controller requires a lower ΔM_z to achieve the same control effect as the SOSM and FOSM controllers. In summary, based on the above analysis and discussion, it can be concluded that the ASOSM controller will exhibit better performance than the FOSM and SOSM controllers.

C. Ramp Steer Tests

The closed-loop simulation test of the controller relies on the performance of CarSim's driver model. In order to eliminate the influence of the driver model on the evaluation results, the performance of the controller is further verified in the ramp steer tests. The controller parameters are as shown in Table II, $V_x =$

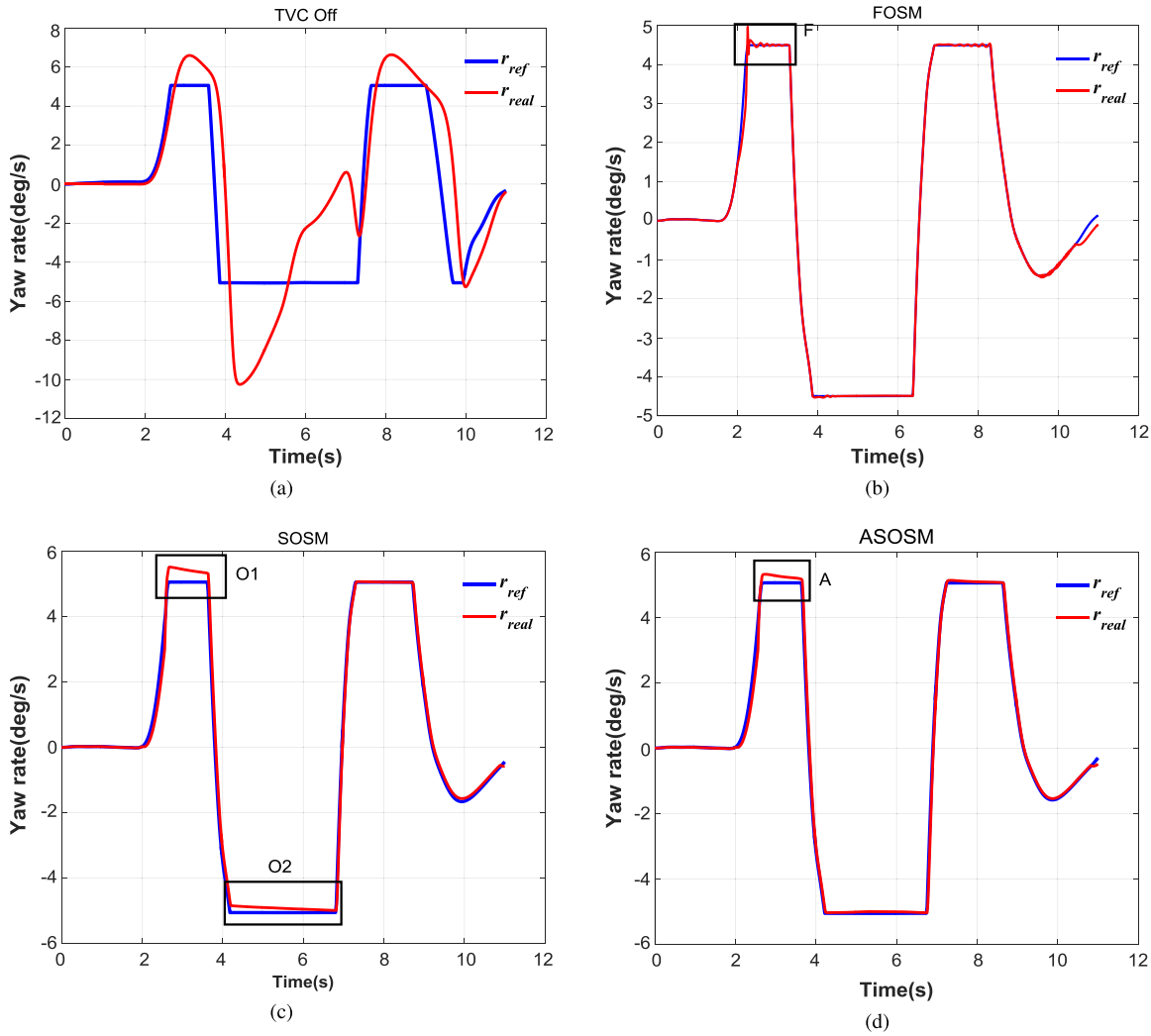

Fig. 11. Yaw rate (γ) evaluated during DLC tests for different controllers.

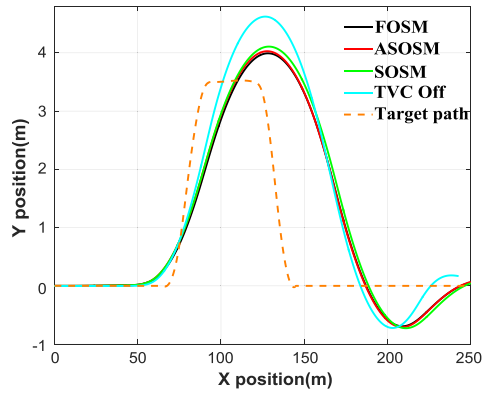

Fig. 12. Vehicle trajectory during DLC tests for different controllers.

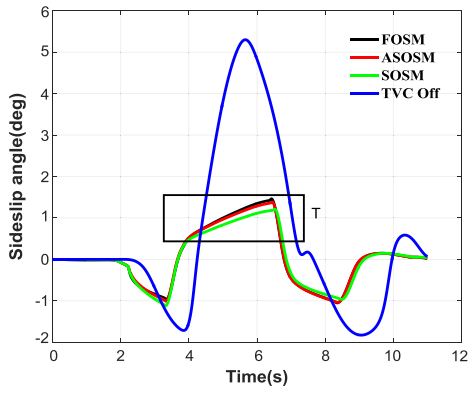

Fig. 13. Sideslip angle (β) during DLC tests for different controllers.

100 km/h, $\mu = 0.5$ are set. The steering wheel angle input to the vehicle is shown in Fig. 16 [39].

The control result of the yaw rate is shown in Fig. 17. For SOSM, the overshoot of the control process is large when the tire force is saturated (F1 in the Fig. 17b). In comparison, even if the tire works in a non-linear region, ASOSM can guarantee a high following accuracy of the yaw rate. For FOSM, the control strategy cannot avoid the chattering phenomenon caused by the

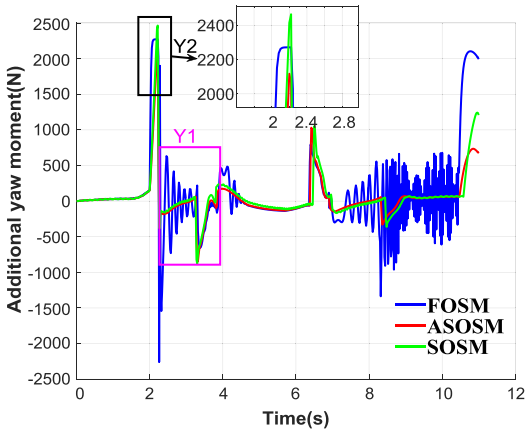

Fig. 14. Additional yaw moment (ΔM_z) during DLC tests for different controllers.

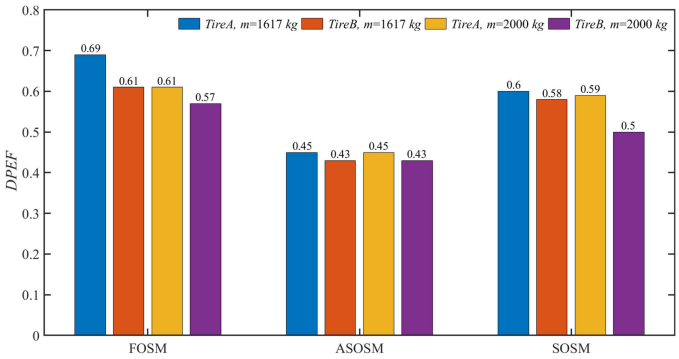

Fig. 15. $DPEF$ values during DLC tests for different controllers.

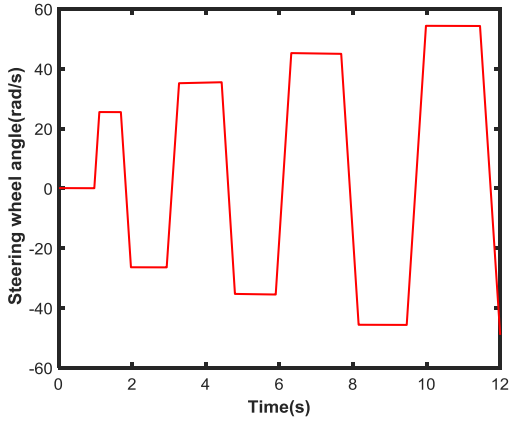

Fig. 16. Steering wheel angle.

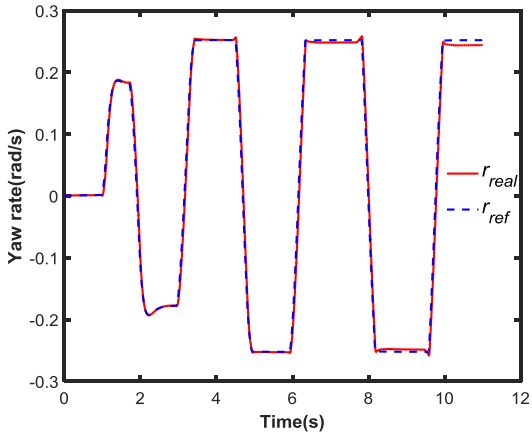

(a) Yaw rate (r) evaluated during ramp steer test for ASOSM

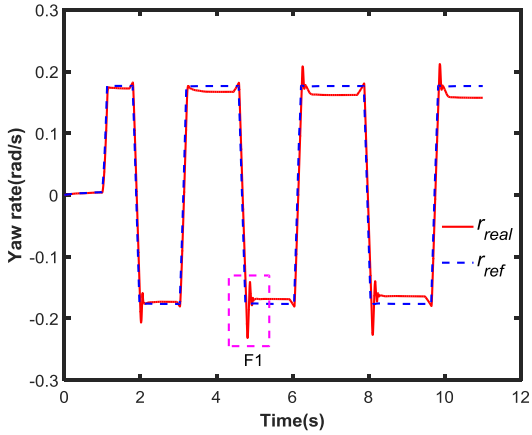

(b) Yaw rate (r) evaluated during ramp steer test for SOSM

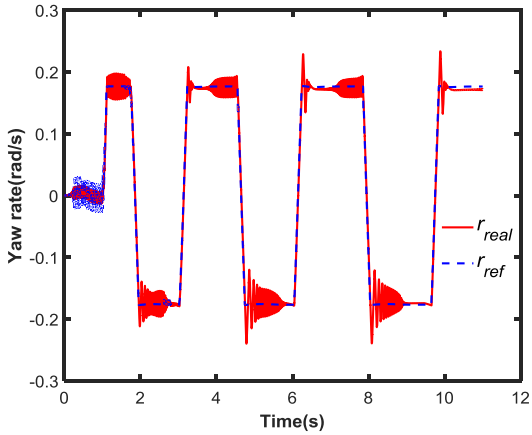

(c) Yaw rate (r) evaluated during ramp steer test for FOSM

Fig. 17. Yaw rate (r) evaluated during ramp steer tests for different controllers.

system state frequently crossing the sliding surface. Therefore, ASOSM has the best control effect in the three controllers.

Curves of the additional yaw moment ΔM_z are depicted in Fig. 18. In order to calculate the maximum additional yaw moment required to achieve the desired control effect, it is assumed that the motor torque is infinite. The FOSM controller output has a large peak value and chattering, and the maximum value of ΔM_z is approximately 21000 N (F2 in the Fig. 18). In contrast, the maximum values of ΔM_z for the ASOSM and SOSM controllers are 1701 N (F3 in the Fig. 18)and 14900 N (F2 in the Fig. 18), respectively, and ΔM_z changes smoothly. In other words, the ASOSM controller can reduce the requirement of the peak output torque of the actuator and solve the chattering problem of the FOSM controller.

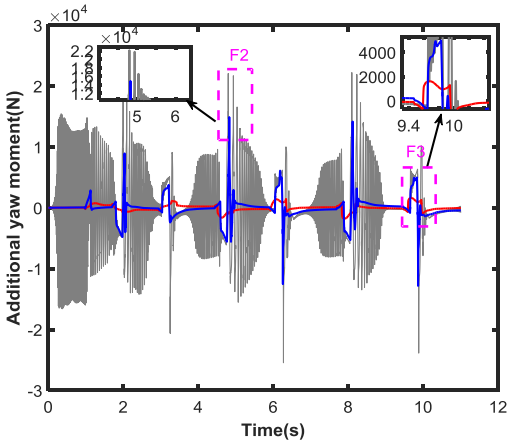

Fig. 18. Additional yaw moment (ΔM_z) during ramp steer tests for different controllers.

V. Conclusion

The goal of this study was to develop an adaptive and robust controller to improve vehicle maneuverability and stability based on TVC without changing the structure of the mechanical system. Adopting the steering characteristics of a 2DOF vehicle model as the ideal steering characteristics, the target cornering response was designed by sets of second-order transfer function parameters, K_{Tar}, ω_{nTar} and ζ_{Tar}. Then, given the many types of disturbance or uncertainty and the chattering problem associated with applying first-order sliding mode control, a robust adaptive second-order sliding mode control method based on backstepping was proposed. The disturbance, including system uncertainties and external disturbance, was approximated by an adaptive law, allowing the sliding surface to approach a given trajectory in a finite time.

Based on this approach, DLC under high-adhesion road conditions was utilized to verify that the bandwidth of the vehicle transient response could be improved by 21% when $\rho = 0$. Compared with the case in which the TVC is turned off, the driver could use a smaller steering angle to more closely follow the target path through the use of TVC. This ability not only improved vehicle maneuverability but also increased driving pleasure. In addition, the suppression of the sideslip angle could be adjusted by changing K_{Tar}, $\omega_{nTar}\zeta_{Tar}$ and ρ, providing the possibility for a personalized control scheme that considers driving style. To further validate the robustness of ASOSM control, a dimensionless performance evaluation weighting function was established to compare and evaluate the performance of FOSM, SOSM, and ASOSM controllers. In the case of DLC under low-adhesion road conditions, the vehicle mass and tire type were varied while maintaining the same control parameter. The simulation results indicated that the ASOSM and SOSM controllers were insensitive to vehicle mass and tire type, implying their robustness to such disturbances. More importantly, the ASOSM controller was consistently able to achieve the minimum $DPEF$ value, whether changing the tire parameters or the weight of the vehicle. When maintaining the same control precision as the SOSM and FOSM controllers, the ASOSM controller required a lower ΔM_z because of the use of an adaptive law. In summary, the results demonstrated that the proposed controller for enhancing vehicle maneuverability and stability is effective and applicable to any drive that can generate a direct yaw moment.

Future studies will address the development of a personalized controller design for comprehensive consideration of improving vehicle maneuverability and stability under different driving styles based on the adaptive torque vector control concept formulated in this study.

References

[1] Y. Huang, A. Khajepour, M. Khazraee, and M. Bahrami, "A comparative study of the energy-saving controllers for automotive air-conditioning/refrigeration systems," *J. Dyn. Syst. Meas. Control*, vol. 139, no. 1, Oct. 2016, Art. no. 014504.

[2] Y. Huang *et al.*, "A review of power management strategies and component sizing methods for hybrid vehicles," *Renew. Sustain. Energy Rev.*, vol. 96, pp. 132–144, Nov. 2018.

[3] S. Ding, L. Liu, and W. X. Zheng, "Sliding mode direct yaw-moment control design for in-wheel electric vehicles," *IEEE Trans. Ind. Electron.*, vol. 64, no. 8, pp. 6752–6762, Aug. 2017.

[4] J. Ghosh, A. Tonoli, and N. Amati, "A torque vectoring strategy for improving the performance of a rear wheel drive electric vehicle," in *Proc. IEEE Vehicle Power Propulsion Conf.*, 2015 pp. 1–6.

[5] L. Zhang, H. Ding, Y. Huang, H. Chen, K. Guo, and Q. Li, "An analytical approach to improve vehicle maneuverability via torque vectoring control: Theoretical study and experimental validation," *IEEE Trans. Veh. Technol.*, vol. 68, no. 5, pp. 4514–4526, May 2019.

[6] Q. Lu, A. Sorniotti, P. Gruber, J. Theunissen, and J. De Smet, "H 8 loop shaping for the torque-vectoring control of electric vehicles: Theoretical design and experimental assessment," *Mechatronics*, vol. 35, pp. 32–43, May 2016.

[7] T. Goggia *et al.*, "Integral sliding mode for the torque-vectoring control of fully electric vehicles: Theoretical design and experimental assessment," *IEEE Trans. Veh. Technol.*, vol. 64, no. 5, pp. 1701–1715, May 2015.

[8] R. Annamalai *et al.*, "Development of vehicle yaw stability controller," SAE Mobilus, Tech. Paper 2013-26-0086, Jan. 2013. Accessed: Jul. 12, 2018. [Online]. Available: https://saemobilus.sae.org/content/2013-26-0086.

[9] A. T. Van Zanten, "Bosch ESP systems: 5 years of experience," *J. Passenger Cars: Electron. Elect. Syst.*, vol. 109, pp. 428–436, 2000.

[10] K. Sawase, Y. Ushiroda, and T. Miura, "Left-right torque vectoring technology as the core of Super All Wheel Control (S-AWC)," Mitsubishi Motors, Tokyo, Japan, Tech. Rev. No. 18, 2006.

[11] H. Yu, W. Liang, M. Kuang, and R. McGee, "Vehicle handling assistant control system via independent rear axle torque biasing," in *Proc. Amer. Control Conf.*, 2009, pp. 695–700.

[12] B. Lenzo, A. Sorniotti, P. Gruber, and K. Sannen, "On the experimental analysis of single input single output control of yaw rate and sideslip angle," *Int. J. Automot. Technol.*, vol. 18, no. 5, pp. 799–811, Oct. 2017.

[13] H. Kanchwala, J. Wideberg, C. B. Alba, and D. Marcos, "Control of an independent 4WD electric vehicle by DYC method," *Int. J. Veh. Syst. Model. Test.*, vol. 10, no. 2, p. 168, 2015.

[14] G. Yin, R. Wang, and J. Wang, "Robust control for four wheel independently-actuated electric ground vehicles by external yaw-moment generation," *Int. J. Automot. Technol.*, vol. 16, no. 5, pp. 839–847, Oct. 2015.

[15] H. Her, Y. Koh, E. Joa, K. Yi, and K. Kim, "An integrated control of differential braking, front/rear traction, and active roll moment for limit handling performance," *IEEE Trans. Veh. Technol.*, vol. 65, no. 6, pp. 4288–4300, Jun. 2016.

[16] X. Ma, P. K. Wong, and J. Zhao, "Practical multi-objective control for automotive semi-active suspension system with nonlinear hydraulic adjustable damper," *Mech. Syst. Signal Process.*, vol. 117, pp. 667–688, Feb. 2019.

[17] Y.-H. Liu, T. Li, Y.-Y. Yang, X.-W. Ji, and J. Wu, "Estimation of tire-road friction coefficient based on combined APF-IEKF and iteration algorithm," *Mech. Syst. Signal Process.*, vol. 88, pp. 25–35, 2017.

[18] B. Zhang, H. Du, J. Lam, N. Zhang, and W. Li, "A novel observer design for simultaneous estimation of vehicle steering angle and sideslip angle," *IEEE Trans. Ind. Electron.*, vol. 63, no. 7, pp. 4357–4366, Jul. 2016.
[19] H. Zhang, G. Zhang, and J. Wang, "Sideslip angle estimation of an electric ground vehicle via finite-frequency $\mathcal{H}_\infty$ approach," *IEEE Trans. Transp. Electrific.*, vol. 2, no. 2, pp. 200–209, Jun. 2016.
[20] Q. Lu *et al.*, "Enhancing vehicle cornering limit through sideslip and yaw rate control," *Mech. Syst. Signal Process.*, vol. 75, pp. 455–472, Jun. 2016.
[21] J. Zhao, P. K. Wong, X. Ma, and Z. Xie, "Chassis integrated control for active suspension, active front steering and direct yaw moment systems using hierarchical strategy," *Veh. Syst. Dyn.*, vol. 55, no. 1, pp. 72–103, Jan. 2017.
[22] L. De Novellis, A. Sorniotti, and P. Gruber, "Optimal wheel torque distribution for a four-wheel-drive fully electric vehicle," *SAE Int. J. Passeng. Cars-Mech. Syst.*, vol. 6, no. 2013-01-0673, pp. 128–136, 2013.
[23] L. De Novellis, A. Sorniotti, and P. Gruber, "Driving modes for designing the cornering response of fully electric vehicles with multiple motors," *Mech. Syst. Signal Process.*, vol. 64–65, pp. 1–15, Dec. 2015.
[24] L. D. Novellis, A. Sorniotti, and P. Gruber, "Wheel torque distribution criteria for electric vehicles with torque-vectoring differentials," *IEEE Trans. Veh. Technol.*, vol. 63, no. 4, pp. 1593–1602, May 2014.
[25] C. Geng, L. Mostefai, M. Denai, and Y. Hori, "Direct yaw-moment control of an in-wheel-motored electric vehicle based on body slip angle fuzzy observer," *IEEE Trans. Ind. Electron.*, vol. 56, no. 5, pp. 1411–1419, May 2009.
[26] S. Zheng, H. Tang, Z. Han, and Y. Zhang, "Controller design for vehicle stability enhancement," *Control Eng. Pract.*, vol. 14, no. 12, pp. 1413–1421, Dec. 2006.
[27] L. Xiong, Z. Yu, Y. Wang, C. Yang, and Y. Meng, "Vehicle dynamics control of four in-wheel motor drive electric vehicle using gain scheduling based on tyre cornering stiffness estimation," *Veh. Syst. Dyn.*, vol. 50, no. 6, pp. 831–846, Jun. 2012.
[28] Z. Shuai, H. Zhang, J. Wang, J. Li, and M. Ouyang, "Combined AFS and DYC control of four-wheel-independent-drive electric vehicles over CAN network with time-varying delays," *IEEE Trans. Veh. Technol.*, vol. 63, no. 2, pp. 591–602, Feb. 2014.
[29] X. J. Jin, G. Yin, and N. Chen, "Gain-scheduled robust control for lateral stability of four-wheel-independent-drive electric vehicles via linear parameter-varying technique," *Mechatronics*, vol. 30, pp. 286–296, 2015.
[30] A. Levant, S. Li, and X. Yu, "Accuracy of some popular non-homogeneous 2-sliding modes," *IEEE Trans. Autom. Control*, vol. 58, no. 10, pp. 2615–2619, Oct. 2013.
[31] Y. Huang, A. Khajepour, H. Ding, F. Bagheri, and M. Bahrami, "An energy-saving set-point optimizer with a sliding mode controller for automotive air-conditioning/refrigeration systems," *Appl. Energy*, vol. 188, pp. 576–585, Feb. 2017.
[32] X. Ma, P. K. Wong, J. Zhao, and Z. Xie, "Cornering stability control for vehicles with active front steering system using T-S fuzzy based sliding mode control strategy," *Mech. Syst. Signal Process.*, vol. 125, pp. 347–364, Jun. 2019.
[33] Y. Chen and J. Wang, "Adaptive energy-efficient control allocation for planar motion control of over-actuated electric ground vehicles," *IEEE Trans. Control Syst. Technol.*, vol. 22, no. 4, pp. 1362–1373, Jul. 2014.
[34] J. Wang and R. G. Longoria, "Coordinated and reconfigurable vehicle dynamics control," *IEEE Trans. Control Syst. Technol.*, vol. 17, no. 3, pp. 723–732, May 2009.
[35] V. Utkin, J. Guldner, and J. Shi, *Sliding Mode Control in Electro-Mechanical Systems*. Boca Raton, FL, USA: CRC Press, 2009.
[36] K. Nam, S. Oh, H. Fujimoto, and Y. Hori, "Design of adaptive sliding mode controller for robust yaw stabilization of in-wheel-motor-driven electric vehicles," *World Electr. Veh. J.*, vol. 5, no. 2, pp. 588–597, Jun. 2012.
[37] D. V. T. Truong, M. Meywerk, and W. Tomaske, "Torque vectoring for rear axle using adaptive sliding mode control," in *Proc. Int. Conf. Control, Autom. Inf. Sci.*, 2013, pp. 328–333.
[38] J. Wang, R. Wang, H. Jing, and N. Chen, "Coordinated active steering and four-wheel independently driving/braking control with control allocation," *Asian J. Control*, vol. 18, no. 1, pp. 98–111, 2016.
[39] L. De Novellis, A. Sorniotti, P. Gruber, and A. Pennycott, "Comparison of feedback control techniques for torque-vectoring control of fully electric vehicles," *IEEE Trans. Veh. Technol.*, vol. 63, no. 8, pp. 3612–3623, Oct. 2014.
[40] L. De Novellis *et al.*, "Direct yaw moment control actuated through electric drivetrains and friction brakes: Theoretical design and experimental assessment," *Mechatronics*, vol. 26, pp. 1–15, Mar. 2015.
[41] T. Kobayashi, E. Katsuyama, H. Sugiura, E. Ono, and M. Yamamoto, "Direct yaw moment control and power consumption of in-wheel motor vehicle in steady-state turning," *Veh. Syst. Dyn.*, vol. 55, no. 1, pp. 104–120, Jan. 2017.
[42] M. Abe, *Vehicle Handling Dynamics: Theory and Application*. London, U.K.: Butterworth-Heinemann, 2015.
[43] H. Yuan, Y. Gao, and T. J. Gordon, "Vehicle optimal road departure prevention via model predictive control," *Proc. Inst. Mech. Eng. Part J. Automob. Eng.*, vol. 231, no. 7, pp. 952–962, 2017.
[44] E. Velenis, D. Katzourakis, E. Frazzoli, P. Tsiotras, and R. Happee, "Steady-state drifting stabilization of RWD vehicles," *Control Eng. Pract.*, vol. 19, no. 11, pp. 1363–1376, Nov. 2011.
[45] H. Pacejka, *Tire and Vehicle Dynamics*. Amsterdam, The Netherlands: Elsevier, 2005.
[46] H. Yuan, X. Sun, and T. Gordon, "Unified decision-making and control for highway collision avoidance using active front steer and individual wheel torque control," *Veh. Syst. Dyn.*, vol. 57, no. 8, pp. 1188–1205, Oct. 2018.
[47] M. Yamakado, J. Takahashi, S. Saito, and M. Abe, "G-vectoring, new vehicle dynamics control technology for safe driving," *Hitachi Review*, vol. 58, no. 7, p. 347, 2009.
[48] H. Zhang, G. Zhang, and J. Wang, "Observer design for LPV systems with uncertain measurements on scheduling variables: Application to an electric ground vehicle," *IEEE/ASME Trans. Mechatron.*, vol. 21, no. 3, pp. 1659–1670, Jun. 2016.
[49] H. Zhang, G. Zhang, and J. Wang, "Sideslip angle estimation of an electric ground vehicle via finite-frequency approach," *IEEE Trans. Transp. Electrific.*, vol. 2, no. 2, pp. 200–209, Jun. 2016.
[50] S. P. Bhat and D. S. Bernstein, "Finite-time stability of continuous autonomous systems," *SIAM J. Control Optim.*, vol. 38, no. 3, pp. 751–766, Jan. 2000.
[51] Z.-L. Gaing, "A particle swarm optimization approach for optimum design of PID controller in AVR system," *IEEE Trans. Energy Convers.*, vol. 19, no. 2, pp. 384–391, Jun. 2004.

Lin Zhang received the Ph.D. degree in automotive engineering from Jilin University, in 2019. He is currently a Post-Doctoral Fellow with the School of Automotive Studies, Tongji University. His research interest include vehicle control in terms of safety, saving energy, and intelligence, including vehicle dynamics and control, HEV control, and trajectory planning.

Haitao Ding graduated from Jilin University in June 2003 and received the Ph.D. degree in vehicle engineering. He is currently teaching and working with the State Key Laboratory of Automotive Simulation and Control, Jilin University. His research interests include automotive dynamics, automotive chassis dynamics control (ABS, ESP, EHB, chassis-integrated control), new energy vehicle (fuel cell vehicles, hybrid vehicles, pure electric vehicles, four-wheel hub drive electric vehicles) modeling, simulation, and control, automotive electronics common technology (CAN and vehicle bus technology, ECU design, embedded software development, HIL testing), driver modeling, and intelligent vehicle control.

Jianpeng Shi graduated from Jilin University and received the Ph.D. degree in vehicle engineering. He is currently working with the Dongfeng Motor Corporation. His main research interests are in the areas of vehicle dynamics control and autopilot motion control and evaluation.

Yanjun Huang received the Ph.D. degree in 2016 from the University of Waterloo, where he is is a Post-Doctoral Fellow with the Department of Mechanical and Mechatronics Engineering. His research interests include vehicle holistic control in terms of safety, saving energy, and intelligence, including vehicle dynamics and control, HEV/EV optimization and control, motion planning and control of connected and autonomous vehicles, and human–machine co-operative driving. He has published several books and more than 50 papers in journals and conferences. He is serving as an Associate Editor and Editorial Board Member of the *IET Intelligent Transport System*, *SAE International Journal of Commercial Vehicles*, *International Journal of Vehicle Information and Communications*, *Automotive Innovation*, AIME, etc.

Hong Chen (M'02–SM'12) received the B.S. and M.S. degrees in process control from Zhejiang University, Zhejiang, China, in 1983 and 1986, respectively, and the Ph.D. degree from the University of Stuttgart, Stuttgart, Germany, in 1997. In 1986, she joined the Jilin University of Technology, Changchun, China. From 1993 to 1997, she was a Wissenschaftlicher Mitarbeiter with the Institut fuer Systemdynamik und Regelungstechnik, University of Stuttgart. Since 1999, she has been a Professor with Jilin University, where she is presently a Tang Aoqing Professor. Her current research interests include model predictive control, optimal and robust control, nonlinear control, and applications in process engineering and mechatronic systems.

Konghui Guo received the B.S. degree from the Jilin University of Technology, Changchun, China, in 1956. He is currently with the National Automobile Dynamic Simulation Laboratory, Jilin University, Changchun, China. Since 1994, he has been an Academician with the Chinese Academy of Engineering. His research interests include the modeling and simulation of vehicle dynamics, tire dynamics, vehicle handling, and stability. He won seven prizes of Progress in Science and Technology awarded by the Chinese Government and the National Automatic Industry Corporation, China.

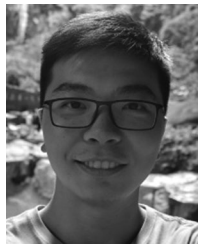

Qin Li received the M.Sc. degree in mechanical engineering from Jilin University, China, in 2016. He is working as the Algorithm Researcher for Intelligent Driving Control System with the GAC R&D Center, China. His main research interests are in the areas of vehicle dynamics control, autopilot motion control, and evaluation.